# Evanescent-field excitation and collection approach for waveguide based photonic luminescent biosensors

E. Rigo · F. J. Aparicio · M. R. Vanacharla ·
S. Larcheri · R. Guider · B. Han · G. Pucker ·
L. Pavesi

**Abstract** A silicon oxynitride channel waveguide based evanescent-field optical transducer is presented for lab-on-chip application. The optical biosensor detects luminescent bioanalytes infiltrated within a reactor well realized across the waveguide. As a main novelty, the sensing mechanism proposed makes use of the evanescent-field propagating in the waveguide to both excite and to collect the fluorescent signal. To understand the chip behavior, its design and collection efficiency were analyzed by finite-difference time-domain simulations in comparison with similar structures differing in the bioreactor thickness and therefore in the excitation and collection mechanisms. It is demonstrated that the best efficiency and performance are reached for the proposed dual evanescent field approach. Characterization of the optical losses and fluorescence measurements from a dye solution infiltrated in the bioreactor well validate the proposed working concept.

## 1 Introduction

Miniaturized sensor devices able to analyze in real-time biological samples are very attractive in a wide range of fields such as: medicine, biology, defense, and food industry [1–3]. One of the most popular approaches for lab-on-a-chip biosensors is based on disposable optical transducers

E. Rigo · F. J. Aparicio · M. R. Vanacharla · S. Larcheri ·
R. Guider · L. Pavesi (✉)
Nanoscience Laboratory, Department of Physics, Università di
Trento, 38123 Povo, Trento, Italy
e-mail: lorenzo.pavesi@unitn.it

B. Han · G. Pucker
CMM-APP, Fondazione Bruno Kessler, 38123 Povo, Trento,
Italy

functionalized with a biological layer (e.g., antibodies, enzymes, DNA, aptamers, and scaffolds [4, 5]) for the specific recognition (typically by immobilization) of a target analyte [1, 6, 7]. Beside the high sensitivity, reliability, immunity to electromagnetic interference, and fast response of the optical techniques, the main advantage of this architecture lies in its selectivity due to the sandwich structure. High selectivity requires the transducer to exclusively respond to those biomolecules immobilized onto the bioreceptor layer. Hence, evanescent-wave sensors, which provide a large-area interaction volume that at the same time is confined to a thickness of just several tens of nanometers, have proved to be of great interest for optical biosensing [6, 8]. Photonic biosensors based on Si compatible materials offer the advantage of exploiting the well-established CMOS micro-fabrication technologies for the development of densely packed multichannel arrays within a single chip. Moreover, these techniques allow for the monolithic integration with the optoelectronic components of the sensor device. Within CMOS compatible materials, silicon oxynitride (SiON), whose refractive index can be adjusted within a rather wide range [9, 10], has proved to be a good candidate for the development of both marked and label-free biosensors, including Mach–Zehnder interferometers, Fabry–Perot and disk resonators, as well as absorption-based biosensors [11–14]. $SiON/SiO_2$ waveguides are particularly interesting for dye labeled biosensors thanks its low optical losses in the UV–visible region, where dye molecules absorb. For instance, propagation losses of ca. 1 dB/cm were reported for waveguides growth by plasma-enhanced chemical vapor deposition (PECVD) [14, 15].

The present paper is concerned with the analysis of an evanescent wave and luminescent-based optical transducer consisting of a SiON channel waveguide where a reactor

well has been carved. Previously, it was proved the detection of a luminescent solution infiltrated into a micrometric reservoir etched throughout the core of a strip waveguide [16]. In this work, the luminescent emission was excited by the laser light which scatters out of the waveguide into the bioreactor, and the detected signal corresponded to the fluorescent emission coupled in the waveguide through its free facet at the other side of the reservoir. As a main difference with this and other luminescent biosensor arrays [17], we propose to employ the evanescent waves which propagate in the reactor well to both excite and collect the luminescent signal. When the reactor well bottom surface is functionalized, this method helps to improve the device selectivity by reducing the thickness of the interaction region. In addition, collection is enhanced since most of the light is emitted toward the high refractive index medium when an emitter is placed near a low-to-high refractive index interface [17–19].

## 2 Device description

The overall layout of the prototype device is shown in Fig. 1a. At first sight, this is similar to the one described in [16], although outstanding differences affecting the sensing mechanism can be found in the bioreactor design. Main components of the optical layer are a set of channel waveguides and the reactor site for the analyte infiltration. Figure 1a also briefly illustrates the two configurations employed to study the optical properties of the structure. In the straight configuration, a laser beam ($I$) is butt-coupled into the input waveguide and transmitted toward the bioreactor, where the luminescent emission is eventually excited and coupled back into the structure. Thereupon, the
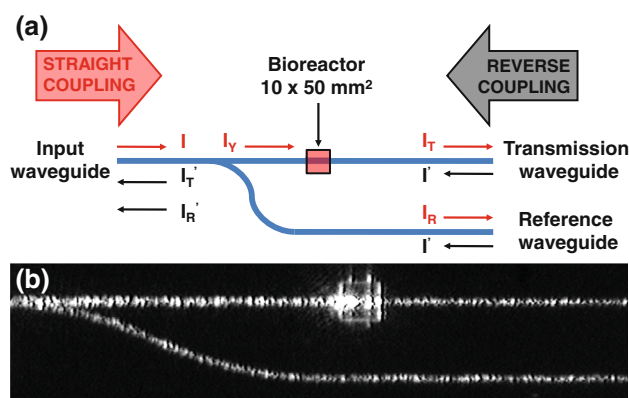
transmitted excitation beam ($I_T$) and the luminescent emission propagate up to the transmission waveguide's output where both signals can be simultaneously detected. The structure also includes a $Y$ splitter before the bioreactor. Thus, the reference branch ($I_R$) allows monitoring the stability of the excitation beam and the reproducibility of the alignment independently of the absorption losses caused by the bioreactor content. Figure 1b shows an image recorded during one of the straight configuration experiments. The scattering signal allows clearly identifying the same layout as depicted in Fig. 1a. In a reverse scheme, the input beam ($I'$) is coupled into the transmission or reference waveguides being $I_T'$ and $I_R'$ the respective output signals (see Fig. 1a).

The structures were fabricated in a standard silicon fabrication line by PECVD and low-pressure chemical vapor (LPCVD) deposition processes in combination with 1,100 °C annealing treatments to remove light-absorbing hydrogen bonds, and optical lithography (pattern definition) and dry reactive-ion etching (RIE) for the pattern transfer process. A schematic representation of the longitudinal cross section of the waveguide at the bioreactor region is presented in Fig. 2. This consists of a 3-μm-thick $SiO_2$ buffer layer ($n = 1.45$ @ 630 nm) and a 240-nm-thick $SiO_xN_y$ core layer ($n = 1.85$ @ 630 nm) both deposited by PECVD, and a ~1-μm-thick borophosphosilicate glass (BPSG) top cladding layer ($n = 1.45$ nm @ 630 nm) in this case grown by LPCVD in order to optimize the surface planarity after RIE [20]. Fabrication of bioreactor wells was also carried out by lithography/RIE. Although the present study is devoted to analyze the optical properties of the nonfunctionalized structures, they have been conceived for specific detection of biomolecules by making use of a biorecognition layer. Hence, the whole system was coated with a thin $SiN_x$ film intended to assist further surface functionalization processes for the development of a bioreceptor layer [21]. Both structure design and materials were selected to minimize the optical losses in the visible and near-infrared (NIR) spectral ranges where organic dyes typically emit (600–800 nm). Bioreactor and, consequently,
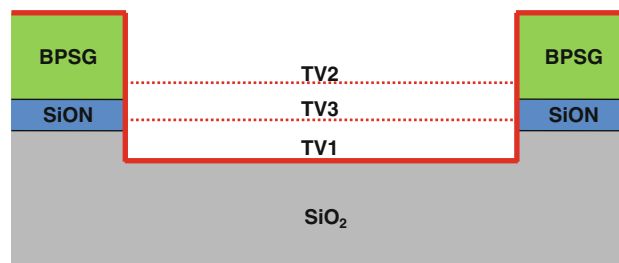


**Fig. 1** **a** Layout of the biophotonic chip. The *blue lines* represent the waveguides, whereas the *red square* corresponds to the region where the bioreactor is etched in the waveguide. *Red* and *blue arrows* correspond, respectively, to the straight and reverse configurations employed to analyze the device's optical properties. **b** Optical image recorded when a laser beam is straightly coupled into the structure



**Fig. 2** Longitudinal cross section of the device at the bioreactor region. The *thin red line* refers to the $SiN_x$ coating. The three different depths of the analyzed bioreactors are represented by *dashed red lines*

**Table 1** Optical losses due to the bioreactor at 670 nm, experimentally and theoretically determined for three filling solutions as indicated in the table

| Sample | Etch depth (μm) | Bioreactor optical losses (dB) | | | | | |
|---|---|---|---|---|---|---|---|
| | | AIR ($n = 1$) | | 2 vol $H_2O$ + 1 vol Glycerol ($n = 1.37$) | | Glycerol ($n = 1.47$) | |
| | | Measured | Simulated | Measured | Simulated | Measured | Simulated |
| TV1 | $1.4 \pm 0.2$ | No signal | 34.0 | $17.9 \pm 5.3$ | 20.4 | $13.4 \pm 2.7$ | 11.2 |
| TV2 | $0.8 \pm 0.2$ | $0 \pm 1$ | 0.0 | $0 \pm 1$ | 0.0 | $0 \pm 1$ | 0.0 |
| TV3 | $1.0 \pm 0.2$ | $6.9 \pm 2.1$ | 8.8 | $3.4 \pm 2.0$ | 4.0 | $2.5 \pm 1.0$ | 1.7 |

The second column refers to the etch depth measured by atomic force microscopy (AFM). Error bars on the experimental data result from repeated experiments

the waveguide dimensions are also dictated by the requirement of a sensing area large enough to be potentially functionalized by a spotter for the specific trapping (i.e., bioreceptor infiltration). Therefore, a 50 × 50 μm bioreactor site was selected, and a waveguide width of 10 μm was chosen to interact with a representative area of the bottom surface of the bioreactor.

According to the general scheme presented in Figs. 1 and 2, three different types of samples were fabricated. They differ in the depth of the bioreactors well (Table 1 and Fig. 2), which was selected to identify the most suitable mechanism for on-chip biosensing applications. In sample named TV1, both the top cladding and the core were completely removed. Sample named TV2 was exposed to a short etching process that did not completely remove the top cladding. Finally, in case of sample named TV3, the etching process was adjusted to completely remove the top cladding and just partially affect the waveguide core, thus preserving a thin core layer of ∼ 80 nm of thickness. It is important to stress that the TV3 core layer was partially etched intending to increase the intensity of the evanescent field out of the waveguide structure. Therefore, three different situations in terms of the interaction between the guided modes and the bioreactor content are tested and analyzed. In the bioreactor TV1, the incoming excitation signal propagates out of the waveguide and, likely, it diffuses all over the bioreactor volume. This is similar to [16]. On the contrary, in the bioreactor of the TV2 sample, herein included as reference, the optical propagating field is well confined in the waveguide core and minimal interaction with the bioreactor content is expected. Finally, bioreactor TV3 represents an intermediate situation where the optical field still propagates through the thinned waveguide core, but its evanescent tail spills out in the detection region. To understand the working principle of these different configurations, we have systematically simulated them by using a commercial parallel 3D finite-difference time-domain (FDTD) software to solve the Maxwell equations [22, 23].

## 3 Bioreactor optical losses

In a first study, the optical losses in the bioreactor well have been both theoretically and experimentally analyzed at 670 nm (pigtailed laser diode). In these studies, three situations were investigated: empty reactor ($n = 1$), reactor filled with a diluted water/glycerol solution (1:2 vol, $n = 1.37$), and reactor filled with glycerol ($n = 1.47$).

Insertion losses due to the bioreactor well were determined as the ratio $I_T/I_Y$, where $I_Y$ and $I_T$ are the signal intensities before and after the bioreactor well, respectively (see Fig. 1a). The intensity $I_T$ is straightforwardly measured at the output of the transmission waveguide, whereas $I_Y$ has to be calculated from the splitting ratio of the Y junction. Since preliminary experiments revealed that the optical losses along the TV2 bioreactor are negligible and independent of the bioreactor content, this reference sample was used to characterize the Y junction. This required conducting a set of reverse coupling experiments (cf. Fig. 1a and Section II) to determine the propagation losses along the different waveguide branches. From these analyses, it determined a splitting ratio $I_Y/I_R = 1.2$ for sample TV2. This splitting ratio value was also assumed for the other samples since all of them have the same design and were fabricated in the same growth run, just differing in the bioreactor etching process.

Experimental and theoretical values of the optical losses in the bioreactor are summarized in the Table 1 for the various bioreactor contents. Experimental data show that the losses follow the sequence TV1 > TV3 > TV2, being negligible for sample TV2. This is expected since a complete removal of the waveguide occurred in TV1, whereas a partial etching of the same was done in TV3, and only a shallow etch of the cladding was observed in TV2. Remarkably, despite that in structure TV3, the etching process reaches the waveguide core and the 50-μm length of the bioreactor well, optical losses have a maximum value of only 7 dB. In addition, the bioreactor optical losses can be significantly reduced by controlling the refractive index of
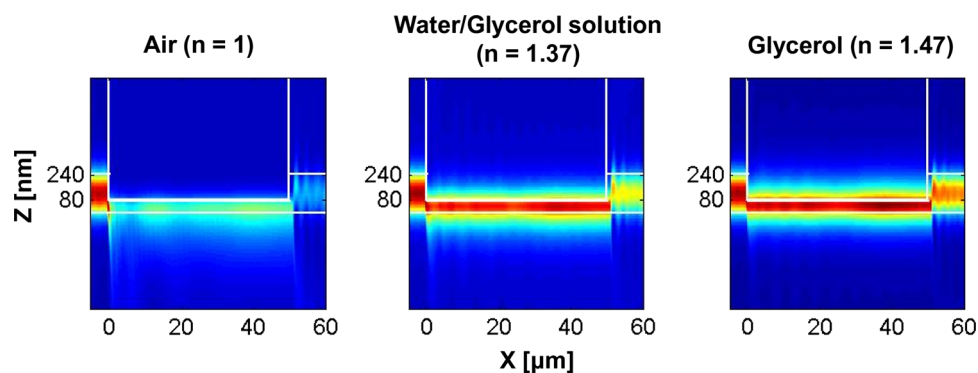
**Fig. 3** Electromagnetic field profiles for a wavelength of 670 nm and TE polarization of the propagating optical mode across the TV3 bioreactor (side view of the 3D simulation) for different bioreactor contents. The *white lines* represent the different geometrical structures. The *Z* values refer to the overall *thickness* of the waveguide out of the bioreactor and the waveguide *thickness* in the bioreactor region

the filling solution reaching a value of 2.5 dB in case of a glycerol. This trend, also observed in sample TV1, is likely accounted for by both the increase of the optical mode confinement in the waveguide and the reduction of the Fresnel losses at the waveguide/reactor interfaces [24, 25].

Simulation is then used to reproduce the experimental results, as well as, to determine the best design for biosensing applications. Since the experimental measurements have been conducted by using unpolarized light, the overall optical transmission across the bioreactor has been calculated as the arithmetic mean of the transmission values obtained from two independent simulations, one for the TE and one for the TM modes. Optical losses obtained by this approach reasonably agree with the experimental values validating the experimental procedure and the simulation approach. Mode profiles along bioreactor TV3 are presented in Fig. 3. Comparison of the images in this figure confirms that the bioreactor content regulates the mode confinement in such a way that the larger the refractive index contrast between the filling medium and the waveguide core, the higher the confinement of the propagating mode. In turn, this effect explains the decrease of the optical losses with the refractive index. Additionally, these results show that when the bioreactor TV3 is filled with a $H_2O$/Glycerol solution or with Glycerol, the evanescent field penetrates deep into the solution and reaches significant intensities at several nanometers out of the core.

## 4 Evanescent-wave excitation and collection

### 4.1 Theoretical simulations

The main object of the present work is to study the possibility of employing the evanescent wave propagating through a channel waveguide to simultaneously excite and collect the luminescent emission from the surrounding dye

molecules, as well as to analyze the thickness of the interaction region, a critical parameter for biosensing applications. With this purpose, theoretical simulations have been carried out by considering the fundamental mode and a bioreactor well filled with water.

Figure 4a shows the optical mode fraction along a virtual 10-nm-thick layer at the center of the waveguide core of sample TV1 (see the inset in the figure). The choice of the thickness is dictated by the typical size of the fluorophore/bioanalyte complexes used for biosensing [26]. The optical mode fraction is defined as the optical power carried by the mode in the layer versus the overall optical power of the mode. Since the optical mode diffracts out when entering into the bioreactor, the optical mode fraction is not constant along the *X* axis, but it rapidly decreases reaching one half of its initial value after a few hundreds of nanometers. In contrast, in the structure TV3, which partially preserves the core layer, the confinement factor of the optical mode in the waveguide core is almost constant in the *X* direction. This allows an easy calculation of the optical power confined within the 10-nm-thick virtual layer as a function of the distance *d* from the bottom of bioreactor TV3 (Fig. 4b). As expected, the relative intensity of the evanescent field exponentially decreases with *d*, from a maximum value of ∼3 %. Note that, for this structure, the penetration depth of the evanescent field, defined as the distance at which the field intensity decays by a factor of 1/e [8], is <90 nm. These results illustrate the capacity of the evanescent mode to preferentially excite those molecules close to the waveguide core. This contrasts with those systems like sample TV1 where the excitation beam is diffracted at the waveguide/bioreactor interface or other approaches where the whole reservoir is illuminated. In this regard, the comparison reported in Fig. 4 indicates that TV3 presents the best perspectives for the homogeneous excitation of a layer of fluorophore-tagged molecules immobilized on the bottom of the bioreactor.
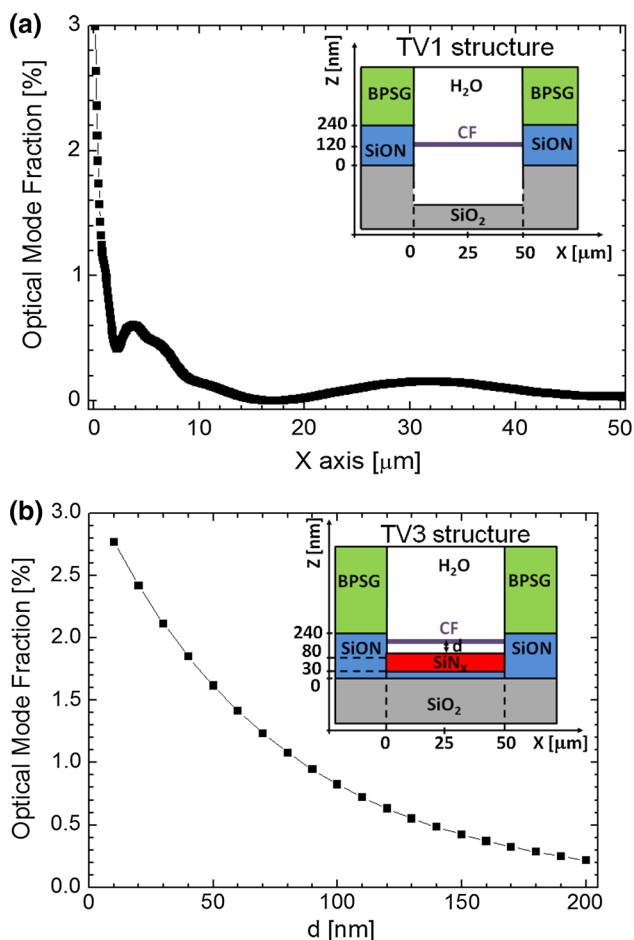
**(a)**

**(b)**

**Fig. 4** Excitation efficiency of the TV1 and TV3 bioreactors at 670 nm. The insets, respectively, show the longitudinal cross section of the two simulated structures. **a** Fraction of the optical mode power along a 10-nm-thick layer centered with respect to the waveguide core, as a function of the distance $X$ from the waveguide/bioreactor interface of structure TV1. **b** Fraction of the optical mode power confined within a 10-nm-thick layer for different heights $d$ from the bottom of the TV3 bioreactor



**(a)**

**(b)**

**Fig. 5** Collection efficiency of the TV3 bioreactor at 740 nm (dye emission wavelength). **a** Collection efficiency of the emitted optical power from an incoherent and isotropic single dipole located at the center of the bioreactor ($X$ axis) as a function of the distance $d$ from the bioreactor bottom surface. The inset shows the sketch of the simulated structure, where the *dashed line* corresponds to the evanescent field profile. **b** The same parameter as a function of the dipole position along the waveguide axis ($X$ direction). Each curve corresponds to different heights $d$

In order to quantitatively determine the efficiency of the structures on the detection of a luminescent marker, the simulation method was modified. For the luminescent analyses, a test fluorophore is placed in several points of the reactor and the emission coupled to the transmission waveguide is calculated by FDTD. The emitting dye molecule is modeled as an isotropic, unpolarized, and incoherent point dipole source. Since our FDTD software only simulates point dipoles with fixed orientation and polarization, several simulations with different dipole orientations are combined and averaged at a fixed dipole position. Finally, the signal in the transmission waveguide resulting from the emission of the dipole is determined at a distance of 10 μm by calculating the resulting intensity of the optical mode in the plane (line T in the insets in Figs. 5a and 6). This signal is normalized to the total
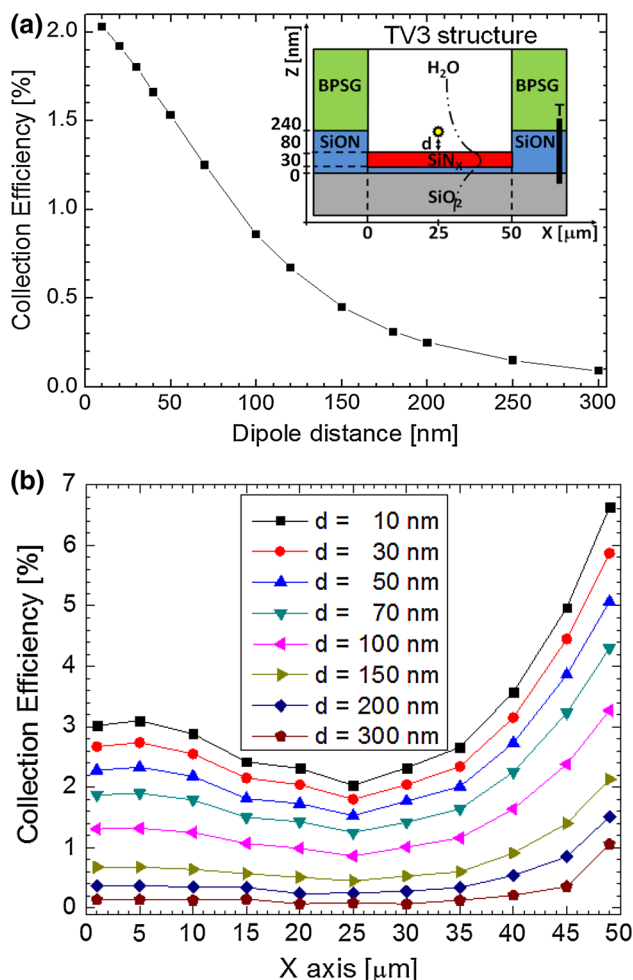
optical power emitted by the dipole obtaining the hereafter denominated collection efficiency. A study of the collection efficiency as a function of the height $d$ from the bottom of bioreactor TV3 is reported in Fig. 5a. Note that, for these simulations, a grid resolution of 10 nm was used and that the dipole is excited with the same rate, independently of its position. Contrary to naïf expectation, the collection efficiency curve is not peaked for a dipole height of 80 nm, the position at which the emission from the dipole best illuminates the free part of the transmission waveguide facet. On the contrary, the collection efficiency follows the profile of the guided modes' evanescent field (compare Fig. 5a and the evanescent-field profile shown in the inset) despite the homogeneous excitation as a function of
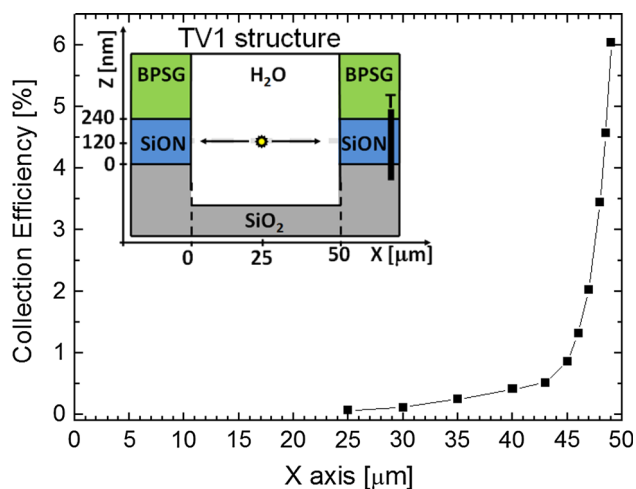
**Fig. 6** Collection efficiency as a function of the dipole position along the waveguide axis (X axis) for the TV1 structure at 740 nm (dye emission wavelength). The simulations were realized at a fixed vertical position corresponding to the center of the waveguide. The inset schematically shows the range of dipole positions

d. Thus, the collection efficiency exponentially decreases with d, having an interaction length (i.e., 1/e distance) of ~110 nm. This behavior suggests that the luminescent signal in the transmission waveguide due to the dipole at the middle of the bioreactor ($X = 25$ μm) is originating from the emitted light coupled through the evanescent tail of the optical-guided mode. At this dipole position, the luminescent signal in the transmission waveguide is not due to the illumination of free facet of the waveguide. This is explained by the fact that the emission of a dipole is influenced by the local photon-mode density. Indeed, the Fermi golden rule states that the spontaneous radiation rate is affected by the photon-mode density which in turn is determined by the dielectric environment. Thus, as it was experimentally reported and theoretically analyzed [18, 19], the emission from a dipole at the interface of two dielectric materials is not isotropic; and most of the energy is radiated toward the high refractive index material. Figure 5a shows that the collection efficiency follows the dipole's spontaneous emission rate which in turn is affected by the waveguide modal structure.

The collection efficiency of bioreactor TV3 as a function of the dipole position along the waveguide axis X is presented in Fig. 5b for several dipole heights. The collection efficiency is almost constant along the first half of the bioreactor length. Meanwhile, it develops along the rest of the bioreactor reaching a maximum value at the proximity of the transmission waveguide's input facet due to the direct coupling of the emission through the free facet of the waveguide. Additionally, at short X, a slight contribution associated with the Fresnel reflection cannot be excluded. According to this interpretation, the coupling efficiency

profiles in Fig. 5b confirm the major role of the evanescent-field coupling, whereas the free facet coupling mechanisms just equal the evanescent-field contribution at the bioreactor/transmission waveguide border. Note that, the evanescent-wave collection allows reaching a 3 % high collection efficiency of the emission of a dipole placed 50 μm far from input facet of the transmission waveguide.

Analogous analyses were realized for the TV1 sample, but in this case as a function of the dipole positions along the X axis and fixing the vertical position of the dipole to the center of the waveguide (Fig. 6). Comparison of these results with those in Fig. 5 indicates the higher efficiency of the TV3 design for the collection of the fluorescent signal and confirms again the importance of the evanescent field in the collection of the fluorescence emission. As a matter of fact, for the TV1 structure, where the emission is only collected through the free waveguide facet, the collection efficiency is lower than 1 % for most of the dipole positions ($X < 45$ μm). Only in the close proximity of the input facet of the transmission waveguide, the collection efficiency increases up to 6 %.

Finally, the overall performance of our devices was evaluated by combining the excitation and collection efficiencies. The X-integral of the product of the collection efficiency (Figs. 5b and 6) and of the confinement factor (cf. Fig. 4) was calculated. This is computed for several distances d from the bottom of the bioreactor. To relate this quantity with the optical power in the input waveguide, the optical losses due to the first interface between the input waveguide and the bioreactor have been estimated to be 2.6 dB for the TV3 structure. Therefore, we determine the device efficiency of our system as the fraction of the emitted power coupled into the transmission waveguide versus the input laser power coupled in the input waveguide and used to excite the dipoles. For the sake of simplicity, it is assumed that the quantum efficiency of the dipoles is 100 %. As illustrated in Fig. 7, the closer the virtual dye layer is to the bioreactor surface, the higher the efficiency of the system. A maximum value of 5 % means that if we excited the bioreactor with a pump laser of 1 mW, then we collect in the output waveguide 0.05 mW of fluorescence signal. From these data, a typical interaction length of ~60 nm was estimated, which is smaller by half of what estimated from Fig. 5. This indicates that by using the evanescent field to both excite and collect the fluorescent signal, the thickness of the sensing region is significantly reduced with respect to similar systems where the evanescent field is exclusively used to collect the fluorescent emission. Since a thin probe region is an important requirement for selective detection purposes, this supports the development of this kind of structures for lab-on-chip biosensing applications. The estimation of the device efficiency for the architecture TV1 when a 10-nm-thick dipole
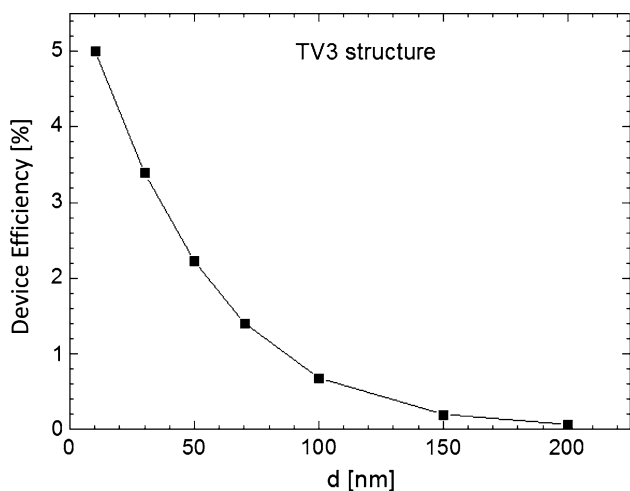
**Fig. 7** Overall device efficiency of the TV3 structure for different distances *d* from the dipole layer to the *bottom* of the bioreactor. The excitation was 670 nm while the emission is analyzed at 740 nm
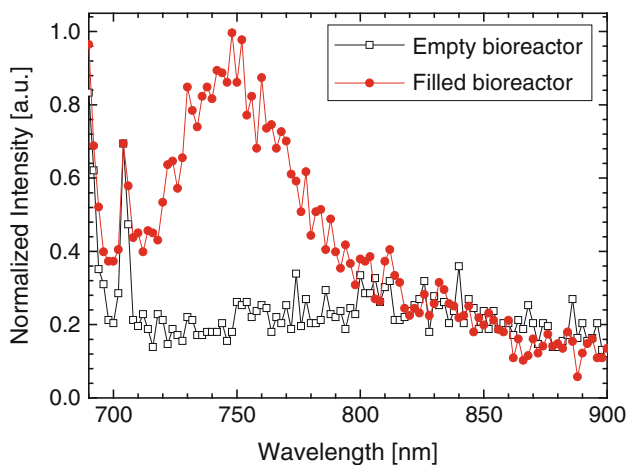


**Fig. 8** Emission spectra before (*black line*) and after (*red line*) infiltrating the TV3 bioreactor with a 100 μM dye solution. The fluorescence emission was excited by coupling a 670-nm laser beam into the input waveguide (cf. Fig. 1)

layer is centered with respect to the waveguide core height yields a device efficiency of only 0.3 %. This small value is due to the combined effect of a short propagation length of the pump beam and of a low collection efficiency which peaks at the transmission waveguide facet.

### 4.2 Detection of a luminescent solution

In order to validate the simulation results, the three structures were experimentally tested for the detection of a luminescent solution. For such experiments, the bioreactors were infiltrated, by using a femtoliter microinfiltrating system from Eppendorf, with water solution of red-emitting dye molecules Furescent Red 7000. In Fig. 8, the emission spectra recorded in sample TV3 before and after

the infiltration of a 100 μM dye solution are presented. When the reactor is empty, only the tail of the laser source ($\lambda = 670$ nm) appears as a weak background signal vanishing at 700 nm (black line). As soon as the droplet of luminescent solution is injected inside the bioreactor, the light guided by the waveguide excites the dye molecules and a fluorescence band is recorded (red line). It is worth noting that during the measurements, the dye solution was continuously injected in the bioreactor in order to compensate the liquid evaporation and maintain the experimental microenvironment as stable as possible. A highly concentrated solution is presented in these analyses, since the purpose of this work is to comparatively study the performance of the different structures but not to determine their detection limit. In this regard, it is important to stress that during our experiments, no fluorescence signal was detected at the output of the TV1 and TV2 transmission waveguides even when using such a high concentration. These results can be taken as a proof of concept validating the dual evanescent-field mechanism of sample TV3, as well as showing the best performance of this architecture in comparison with the ones represented by samples TV1 and TV2.

### 5 Conclusions

An evanescent-field excitation and collection combined approach is analyzed for a channel-waveguide-coupled bioreactor conceived as the optical transducer part of a more complex luminescent biosensor. This simple photonic structure can find applications as integrated optical sensor in the visible–NIR spectral range to detect the presence of fluorescent marked molecules infiltrated within the reactor well. The proposed scheme is compared with the excitation and collection mechanism of a more simple structure where the evanescent field does not play any role. The present study shows the advantages of the dual evanescent-field approach where all the surface of the waveguide section within the bioreactor is used to excite and collect the fluorescence signal. Such design provides a higher sensitivity than the others herein analyzed. Moreover, both excitation and collection efficiencies decrease with the distance between the marked molecules and the bottom surface of the bioreactor. In this regards, our simulations indicate that the combined approach allows decreasing the thickness of the interaction region down to ∼60 nm. Thus, the structure can be used for the selective detection of specific biomolecules after the functionalization of the structure with a suitable biorecognition layer. These characteristics together with the possibilities of the employed CMOS fabrication techniques allow for extending the design to the development of a single-system sensors array

with multianalyte capabilities, by functionalizing each single sensing structure with a specific biorecognition layer.

## References

1. P. Seitz, Optical biochips, in *Biophotonics*, ed. by L. Pavesi, P. Fauchet (Springer, Berlin, 2008)
2. D. Janasek, J. Franzke, A. Manz, Nature **442**, 374-380 (2006)
3. Y. Kostov, G. Rao, Rev. Sci. Instrum. **71**, 4361-4374 (2000)
4. M.F. Templin, D. Stoll, J.M. Schwenk, O. Pötz, S. Kramer, T.O. Joos, Proteomics **3**, 2155-2166 (2003)
5. S.-Y. Seong, C.-Y. Choi, Proteomics **3**, 2176-2189 (2003)
6. V. Passaro, F. Dell'Olio, B. Casamassima, F. De Leonardis, Sensors **7**, 508-536 (2007)
7. P.N. Patel, V. Mishra, A.S. Mandloi, J. Eng. Res. Stud. **1**, 15-34 (2012)
8. R. Kunz, K. Cottier, Anal. Bioanal. Chem. **384**, 180-190 (2006)
9. Y. Lianghong, L. Ming, W. Leszek, S. Weiwei, T. Jun, L. Yicheng, J. Wei, J. Opt. **14**, 085501 (2012)
10. R.M. De Ridder, K. Warhoff, A. Driessen, P.V. Lambeck, H. Albers, IEEE J. Sel. Top. Quantum Electron., **4**, 930-937 (1998)
11. V.L. Paul, Meas. Sci. Technol. **17**, R93 (2006)
12. P.S. Nunes, N.A. Mortensen, J.P. Kutter, K.B. Mogensen, Opt. Lett. **33**, 1623-1625 (2008)
13. D. Klunder, J. Elders, G.-J. Burger, M. Amersfoort, E. Krioukov, C. Otto, H. Hoekstra, A. Driessen, in *Proceedings SPIE 5269, Chemical and Biological Point Sensors for Homeland Defense*, (2004) doi:10.1117/12.515862
14. K.B. Mogensen, P. Friis, J. Hübner, N. Petersen, A.M. Jørgensen, P. Telleman, J.P. Kutter, Opt. Lett. **26**, 716-718 (2001)
15. B. Han, E. Rigo, R. Guider, S. Larcheri, G. Nunzi Conti, M.R. Vanacharla, A. Chiasera, M. Ferrari, L. Pavesi, G. Pucker, G. C. Righini, M. Ghulinyan, in *Proceedings SPIE 8069, Integrated Photonics: Materials, Devices, and Applications, 80690 K*, (2011) doi:10.1117/12.886820
16. A. Cleary, A. Glidle, P.J.R. Laybourn, S. Garcia-Blanco, S. Pellegrini, C. Helfter, G.S. Buller, J.S. Aitchison, J.M. Cooper, Appl. Phys. Lett. **91**, 071123 (2007)
17. F. Baldini, A. Carloni, A. Giannetti, G. Porro, C. Trono, Anal. Bioanal. Chem. **391**, 1837-1844 (2008)
18. C. Burke, O. Stránik, H. McEvoy, B. MacCraith, Planar optical sensors and evanescent wave effects, in *Optical Chemical Sensors*, ed. by F. Baldini, A.N. Chester, J. Homola, S. Martellucci (Springer, Netherlands, 2006)
19. L.U. Polerecky, J. Hamrle, B.D. MacCraith, Appl. Opt. **39**, 3968-3977 (2000)
20. M. Ghulinyan, R. Guider, G. Pucker, L. Pavesi, IEEE Photon. Technol. Lett. **23**, 1166-1168 (2011)
21. F. Cattaruzza, A. Cricenti, A. Flamini, M. Girasole, G. Longo, A. Mezzi, T. Prosperi, J. Mater. Chem. **14**, 1461-1468 (2004)
22. O. Parriaux, G.J. Veldhuis, J. Lightwave Technol. **16**, 573 (1998)
23. "Lumerical Solutions," (Inc. Vancouver U.S., 2010)
24. J.S. Kee, D.P. Poenar, P. Neuzil, L. Yobas, Sens. Actuators B: Chem. **134**, 532-538 (2008)
25. K.B. Mogensen, J.P. Kutter, Electrophoresis **30**, S92-S100 (2009)
26. I. Paribok, G. Zhavnerko, V. Agabekov, Y. Zmachinskaya, A. Yantsevich, S. Usanov, Russ. J. Gen. Chem. **77**, 363-366 (2007)